Lab on a Chip

PAPER

View Article Online
View Journal | View Issue

A solvent resistant lab-on-chip platform for radiochemistry applications†

Cite this: *Lab Chip*, 2014, **14**, 2556

Christian Rensch,*[a] Simon Lindner,[b] Ruben Salvamoser,[a] Stephanie Leidner,[b] Christoph Böld,[a] Victor Samper,[a] David Taylor,[a] Marko Baller,[c] Stefan Riese,[d] Peter Bartenstein,[b] Carmen Wängler[be] and Björn Wängler*[f]

Received 17th January 2014,
Accepted 13th April 2014

DOI: 10.1039/c4lc00076e

www.rsc.org/loc

The application of microfluidics to the synthesis of Positron Emission Tomography (PET) tracers has been explored for more than a decade. Microfluidic benefits such as superior temperature control have been successfully applied to PET tracer synthesis. However, the design of a compact microfluidic platform capable of executing a complete PET tracer synthesis workflow while maintaining prospects for commercialization remains a significant challenge. This study uses an integral system design approach to tackle commercialization challenges such as the material to process compatibility with a path towards cost effective lab-on-chip mass manufacturing from the start. It integrates all functional elements required for a simple PET tracer synthesis into one compact radiochemistry platform. For the lab-on-chip this includes the integration of on-chip valves, on-chip solid phase extraction (SPE), on-chip reactors and a reversible fluid interface while maintaining compatibility with all process chemicals, temperatures and chip mass manufacturing techniques. For the radiochemistry device it includes an automated chip-machine interface enabling one-move connection of all valve actuators and fluid connectors. A vial-based reagent supply as well as methods to transfer reagents efficiently from the vials to the chip has been integrated. After validation of all those functional elements, the microfluidic platform was exemplarily employed for the automated synthesis of a Gastrin-releasing peptide receptor (GRP-R) binding the PEGylated Bombesin BN(7–14)-derivative ([^{18}F]PESIN) based PET tracer.

Introduction

Positron Emission Tomography (PET), a "molecular imaging" technology, is a medical imaging technique that utilizes radioactively labelled molecules (PET tracers) that are tailored to interact with biological processes *in vivo*.[1] After injection into the patient, a PET tracer shall accumulate at areas of interest according to its pharmacokinetic properties. Subsequently, the resulting radioactivity distribution in the patient is measured utilizing a PET scanner, today commonly in combination with anatomic image acquisition from computer tomography (PET/CT) or magnetic resonance imaging (PET/MR).

Regardless of the imaging device utilized, the majority of the resulting diagnostic information is determined by the biological or biochemical function of the PET tracer, indicating for example areas of increased or decreased sugar metabolism ([^{18}F]Fludeoxyglucose), high cell membrane production (*e.g.* [^{18}F]Cholin) or receptor specific binding (*e.g.* [^{18}F]Fallypride for dopamine D2/D3 receptors). Therefore, new PET tracers are currently under development by academic and industrial entities. A major challenge associated with the transfer of this increasing variety of radioactively labelled molecules into clinical practice is the infrastructural burden associated with the synthesis of PET tracers. Today, this step is performed by automated synthesis devices ("synthesizers") utilizing conventional valves, tubing and glass vessels inside a lead shielded work space ("hot cells"). One hot cell can result in a weight of 8 tons while requiring a class C clean room environment of approx. 1000 litres according to regulatory requirements. This leads to significant costs and infrastructural constraints for PET site erection, modification and routine PET tracer

[a] *GE Global Research, Freisinger Landstrasse 50, 85748 Garching bei Munich, Germany. E-mail: rensch@ge.com; Fax: +49 89 5528 3181; Tel: +49 89 5528 3613*
[b] *University Hospital Munich, Department of Nuclear Medicine, Ludwig Maximilians University, 81377 Munich, Germany*
[c] *Department of Biomedical Sciences in Micro- and Nanotechnology, University of Applied Sciences Kaiserslautern – Zweibrücken, Amerikastr. 1, 66482 Zweibrücken, Germany*
[d] *GE Healthcare, Schaimburgstraße 3, 48145 Münster, Germany*
[e] *Biomedical Chemistry, Department of Clinical Radiology and Nuclear Medicine, Medical Faculty Mannheim of Heidelberg University, 68167 Mannheim, Germany. E-mail: bjoern.waengler@med.uni-heidelberg.de; Tel: +49 621 383 2067*
[f] *Molecular Imaging and Radiochemistry, Department of Clinical Radiology and Nuclear Medicine, Medical Faculty Mannheim of Heidelberg University, 68167 Mannheim, Germany*

† Electronic supplementary information (ESI) available. See DOI: 10.1039/c4lc00076e

production. Furthermore, state of the art synthesizers utilize reagent volumes from several hundred microliters to a few millilitres for reasons of practicality. These volumes are several orders of magnitude above the theoretically required amount, since PET tracers are functional in nanomolar quantities of the radioactively labelled molecules.

Intuitively, microfluidic technology was introduced to the field, targeting a down-scaling of synthesizers to achieve a reduced shielding size and weight as well as more efficient chemical processing.[2–13] For about one decade, numerous microfluidic PET tracer synthesis setups have been described including commercially available capillary-based microfluidic synthesis platforms,[14–16] as well as lab-on-chip devices.[17–22] Significant improvements to PET tracer synthesis were demonstrated such as reduced reaction times due to fast heat transfer and high surface to volume ratios in microfluidics, low consumption of potentially expensive reagents, fast optimization of reaction conditions and low volume processing of radioactivity levels sufficient for practical use.[23–48]

However, the large characteristic dimensions (including all hardware periphery) of the microfluidic setups presented as well as the system complexity exposed to the operator have remained two major obstacles towards routine use. Furthermore, PDMS-based chip designs that capitalize on highly integrated valves have been questioned due to the incompatibility of PDMS to fluoride-18 based radiochemistry.[49]

This study tackles those challenges and presents a radiochemistry system that unites all technical elements required for a simple PET tracer synthesis in one compact, easy to use device. First and foremost this includes a chip material with full compatibility to process reagents and temperatures. Second, the utilization of this material is enabled by a chip manufacturing technology with potential for economy of scale. Third, functional elements required for the execution of the synthesis workflow are implemented into the chosen chip material technology. These functional elements are on-chip microfluidic reactors, on-chip fluid and gas control by means of on-chip valves and associated compact off-chip valve actuators, on-chip solid phase exchange (SPE) and a connector interface between the chip and the hardware periphery. To improve ease of use, the chip to hardware interface is designed for full automation, enabling seamless chip loading and unloading in a single motion. Reagents are transferred from low dead-volume vials across the interface by means of gas pressure driven fluid transport. All described elements are integrated into a hardware assembly that has potential for compact shielding architectures. The functionality of the platform is exemplarily demonstrated by the complete synthesis of a Polyethylenglycol-derivatized (PEGylated) Bombesin BN(7–14)-derivative ([^{18}F]PESIN).

Published on 14 April 2014.

Materials and methods

Fundamental considerations

The ultimate target of synthesizing a PET tracer on a microfluidic system in a routine environment is to provide a PET image to a medical doctor at an acceptable cost.[50] In this context, the most important key figure is "cost per (PET) dose", which rolls up all elements of PET facility installation and operation. Accordingly, cost is critical for the microfluidic synthesizer as a system (*e.g.* reduced installation cost by means of reduced shielding installation) as well as its operation (*e.g.* cost of consumables).

Currently there are two fundamental microfluidic system architectures in radiochemistry: chip-based and capillary-based synthesizers. The advantage of chip-based microfluidic devices is seen in the capability for cross-contamination-free production of various PET tracers in series with no need for manual hardware re-configuration or cleaning between runs and therefore full compliance with regulatory requirements. In this case, the microfluidic chip is replaceable, single-use consumable and comparable to current synthesizers that are utilizing disposable fluid path manifolds ("cassettes") and a set of reagents ("reagent kits") that may be produced in separate or as combined cassettes with integrated reagents (*e.g.* GE FASTlab, GE Healthcare, Liege, Belgium). Today, one cassette and one reagent kit are often used for the synthesis of PET tracer "batches" that serve several patients at once, leading to a reduced contribution of consumables cost to the cost per PET tracer dose.

In contrast, the major application of microfluidic PET tracer synthesizers is seen in the area of small patient groups (<10) that either require PET tracers "on demand" or are located at hospitals with limited connectivity to PET tracer distribution networks, also referred to as "de-centralized" production sites.[7] Hence, the manufacturing cost target for a single microfluidic consumable including reagents has to be expected at a fraction of today's consumables cost. Based on the number of existing PET facilities worldwide and the limited growth of reimbursement for PET, the number of chips required globally per year is estimated to be a few hundred thousand. Both the high cost pressure on consumables and the number of parts per year put significant limitations on the materials and manufacturing methods that can be employed to realize a lab-on-chip consumable that is commercially viable.

Microfluidic chip manufacturing

According to the cost constraints described, a materials study was conducted and published in previous work.[49] From this study, injection mouldable cyclic olefin co-polymers (COCs) were selected. Injection moulding and embossing are cost effective methods for manufacturing of microfluidic parts down to sub-micron geometric accuracy at a low production cycle time per part.[51,52] COC is compatible with many reagents utilized in radiochemistry including strong acids (*e.g.* hydrochloric acid), bases (*e.g.* sodium hydroxide), polar organic solvents (*e.g.* dimethyl sulfoxide, acetonitrile or dimethylformamide) and alcohols (*e.g.* ethanol). Beyond the room temperature Silicon Fluoride Acceptor (SiFA) based radiochemistry employed in this study, COC is compatible

with process temperatures of up to 150 °C such as for the synthesis of the PET tracer, [18F]fluorothymidine ([18F]FLT).[53] COC is further marked by its low raw material cost of around one cent (US) per gram.[49]

COC 6017-S04 (TOPAS® Advanced Polymers GmbH, Germany) was utilized for injection moulding of rectangular blanks (Rodinger Kunststoff-Technik GmbH, Germany) with outer dimensions of 100 mm × 100 mm × 2 mm. A COC 6015 film (TOPAS® Advanced Polymers GmbH, Germany) of 100 μm thickness was obtained to construct on-chip valves. One microfluidic chip (Fig. 1) consists of three separate layers (outer dimensions: each 95 mm × 60 mm × 2 mm), all processed from the moulded blanks. All microfluidic structures on each of the layers are created utilizing a four axis computerized numerical controlled (CNC) milling machine (MDX-540 SA, Roland DGA Corp., USA). During microfluidic chip design, compatibility with injection moulding techniques was assured for all structures on-chip (RKT Rodinger Kunststoff-Technik GmbH, Germany). After milling, all layers including the foil were cleaned and assembled together with the elements for on-chip valve and on-chip resin integration. The assembly process was designed with potential for cost effective pick-and-place automation. After assembly, all chip elements were joined in a single thermal bonding step. No additional cleaning, surface treatment, adhesives, ultrasound nor laser processes were required.

On-chip valve

Due to the need for organic solvent compatibility (*e.g.* dimethyl formamide or dimethyl sulfoxide), common microfluidic valve designs that rely on flexible membrane materials such as PDMS or Viton® are not suitable.[54–58]

The membrane valve developed in this study utilizes a floating FEP disk (DuPont FEP, part no. #536-3996, RS Components GmbH, Germany) encapsulated by the chip substrate (COC 6017) and a 100 μm thick cover membrane (COC 6015).[59] The valve inlet and outlet can be prototyped by utilizing high precision milling techniques and are suitable for injection moulding. Due to the materials (COC and FEP) utilized, the valve is compatible to acids, bases and organic solvents as well as temperatures of up to 150 °C. After assembly and bonding, the valve is normally open (Fig. 1). For valve closure, a spring loaded solenoid driven external plunger is pressed on the COC membrane, driving the FEP disk against the valve seat. This design leads to two fundamental advantages: (a) the contaminated fluid path remains encapsulated within the chip and (b) all valve actuators can be connected and disconnected with the chip in a single automated motion. A total number of 16 independently controllable valves have been integrated into one microfluidic chip.

The valve design was characterized under realistic conditions of use in terms of maximum pressure capability and repeatable performance for 50 opening and closing cycles. The valve leakage rate was determined by a simplified test applying gas pressure to the valve inlet and subsequent observation of bubble formation at the valve outlet.

On-chip resin

The synthesis of PET tracers often requires functional resins for the initial transfer of radioactive fluoride-18 from aqueous to aprotic reaction conditions and for intermediate as well as final product purification. Several techniques have been reported including manual filling of on-chip cavities,[60] on-chip

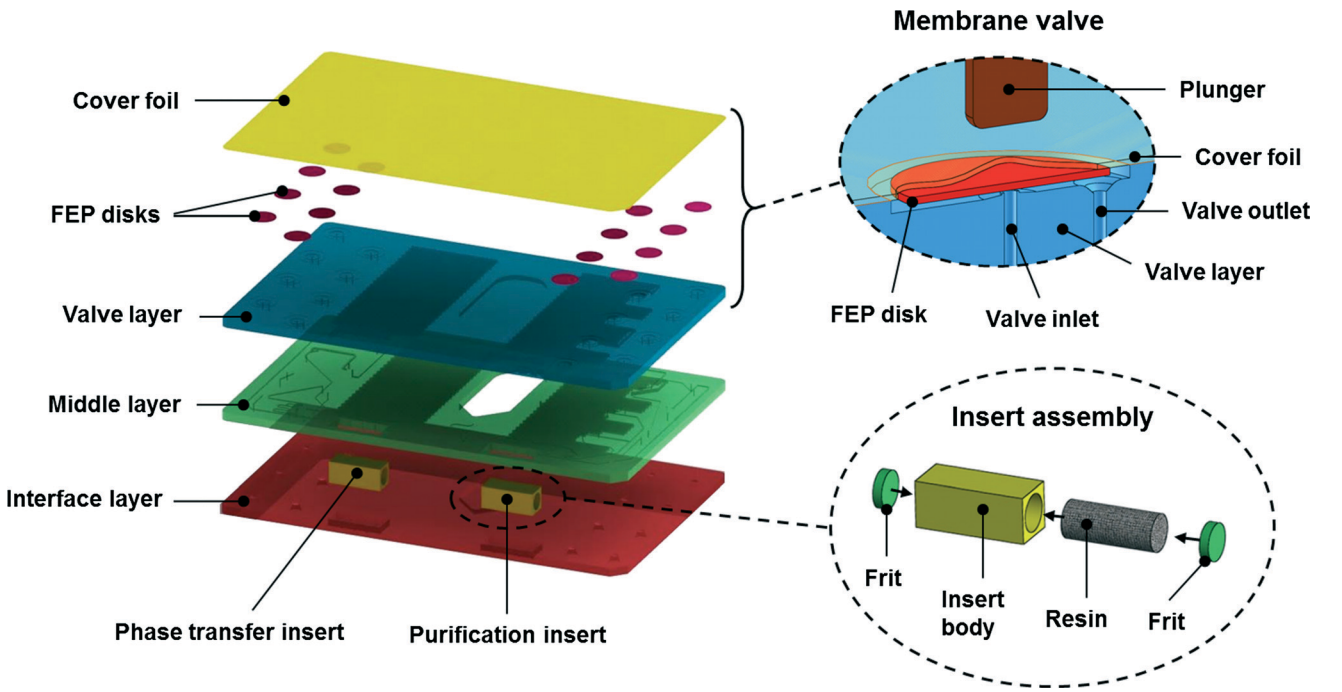

Fig. 1 Schematic of microfluidic chip assembly including the membrane valve and the insert assembly.

trapping of solution suspended beads[19] as well as introduction, photo-initiated polymerization and functionalization of reactive compounds for monolithic on-chip columns.[61] Even though there have been successful efforts to reduce the need for SPE-based process steps by means of electrochemical methods[62–69] or continuous flow microfluidics,[70] the challenge remains for product purification, resulting in custom made microcolumns external to the microfluidic chip.[17,18,71] Future on-chip alternatives may involve periodic microstructures such as pillar arrays[72] as well as functional surfaces. However, all methods described impose challenges on process chemistry, repeatability, compatibility with established synthesis routines, reagent volumes and throughput, manufacturing complexity and economy of scale.

The resin integration method proposed in this work utilizes an insert element that is pre-filled with conventional resins, separating the integration workflow into three steps: a) resin transfer to a low-cost carrier element (insert body, compare Fig. 1) by means of conventional filling techniques; b) assembly of the insert element into a recess on chip; and c) connection to the on-chip fluid path during chip bonding.

The insert bodies are of simple geometry and milled from COC 6015 (TOPAS® Advanced Polymers GmbH, Germany), enabling compatibility with all relevant process chemicals, temperatures and low cost injection moulding. The silica-based resin material is extracted from the respective standard cartridges and manually transferred to the COC 6015 insert bodies creating phase transfer inserts and purification inserts. Prior to bonding, the pre-assembled inserts are manually positioned into milled recesses between the three microfluidic chip layers, wherein each insert is slightly smaller in two (X and Y) and larger in one dimension (Z) than the recess. After chip assembly, the COC 6015 insert is thermoformed into the recess during chip bonding. This approach capitalizes on the different glass transition temperatures between COC 6015 (HDT/B = 150 °C) and COC 6017 (HDT/B = 170 °C). The required thermo-forming pressure is provided by the geometric mismatch between the insert and the on-chip recess and has to be adjusted based on the insert size.

The on-chip cartridges can be varied in number, packaged resin size and location on the chip during chip design. For future high volume production, cartridge manufacturing can be standardized and manual assembly steps may be replaced by *e.g.* pick-and-place automation.

Chip interface for liquids and gases

The micro- to macro interface is a known challenge for microsystems and numerous microfluidic connectors that have been described in the literature.[73] However, most solutions are not compatible with the chemicals employed in PET chemistry or are challenging to connect in an automated fashion due to a multi-component design involving O-rings, screws or adhesives.

Conventional high performance liquid chromatography (HPLC) fittings capitalize on the mechanical advantage of a wedge. The same principle is applied to the design presented in this study utilizing conventional conical ferrules (F-142N ETFE ferrules, Techlab GmbH, Germany) which are compressed into conic recesses on the chip.[74] At an on-chip cone opening angle of 42° (recess depth 1.5 mm) a compression force of 20 N between the ferrule and chip was found sufficient to achieve liquid sealing (2-propanol) up to a pressure of 100 bar. In order to compensate for mechanical misalignment during automated chip loading and cross forces resulting from thermal expansion of the chip when operated at elevated temperatures, a compensation mechanism[75] has been implemented (Fig. 2). By this design, sealing is achieved for 16 fluid ports and multiple opening and closing cycles. Similar to the valve actuators, connectivity between the chip and the hardware is achieved in a single automated motion.

Reagent supply and loading

The gold standard for reagent storage in radiochemistry is septa capped glass vials since this method is compatible to long term storage of solvents such as DMSO. Accordingly, reagents at a volume range between 50 μl and 2 ml are provided to the platform from septa capped low dead-volume vials (Certified CD™ Vial, part no. 29307-U, Supelco Analytical, USA). Since conventional Luer adapters show dead volumes >10 μl, the vials are interfaced by a custom built low dead volume connector. Each vial is connected *via* the adapter to the chip interface using a single PEEK capillary line. This line is utilized for gas pressurization of the vial as well as subsequent pressure driven unloading of the reagent to the chip. Only on-chip valves are utilized to switch between vial pressurization and reagent unloading, minimizing the number of transfer lines and the associated interface complexity as well as the risk of leakages.

On-chip reagents are driven by gas pressure, in case accurate metering of flow rates is not required (*e.g.* application of

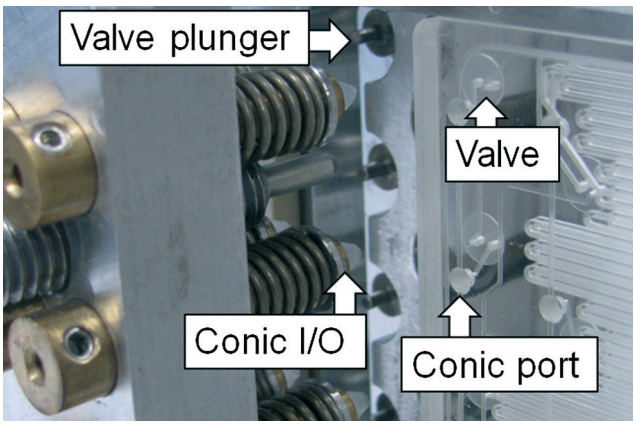

Fig. 2 Detailed view of the chip manifold in the open position with the chip not completely inserted. The conic I/O ports as well as the valve plungers can be connected within a single move to the on-chip valves and conic ports.

aqueous activity to the QMA cartridge). For accurate metering (*e.g.* precise mixing during HEPES buffer dilution), two or more syringe pumps of the control box can be employed utilizing *e.g.* acetonitrile as mediators between the reagents to be controlled on-chip and the syringe pump.

Compact control hardware

The control hardware can be separated into two sub-systems: (1) the chip manifold and (2) the control device (Fig. 3).

This arrangement is chosen with potential for "split-box" or "self-shielded" architectures which provide shielding only to system elements in contact with radioactive reagents, in this case the chip and the surrounding chip manifold.[32] This approach is superior to conventional hot cell designs in terms of weight, space consumption, installation cost and flexibility.

The chip manifold contains the fluid interface with 16 input/output (I/O) ports and the valve actuator assembly (Fig. 4). After manual chip insertion, the valve actuator interface automatically compresses the chip against the fluid interface by means of a motor driven mechanism, enabling a connection of all chip control elements with one move. Heating blocks enabling on-chip process operation at temperatures of up to 150 °C were integrated into the setup but not used in this study.

A mechanism for chip ejection after process completion has been integrated in order to demonstrate the prospect of automated disposal of contaminated chips into shielded waste areas for seamless "back-to-back" operation of consecutive synthesis runs at low radiation exposure to the operator.

The control device contains all control electronics required for on-chip valve actuation, chip loading and unloading and five syringe pumps (Cavro® XCalibur, Tecan Group Ltd., Switzerland) equipped with one 3-port rotary valve each as well as a sensor for on-chip pressure monitoring. The characteristic dimensions of the chip manifold are 250 × 135 × 130 (mm) and of the control box are 270 × 370 × 210 (mm) making the system easily portable to various test sites.

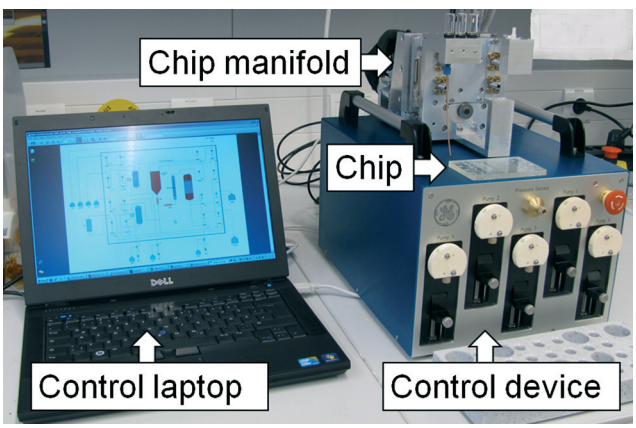

Fig. 3 The microfluidic chemistry platform including the chip manifold, microfluidic chip, control device and laptop.

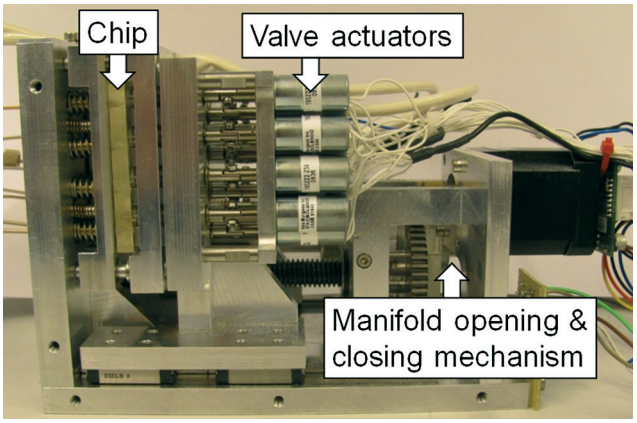

Fig. 4 The chip manifold in the closed position (side view).

A LabVIEW-based software is employed for system control *via* a laptop connected to the control device. The control software separates the synthesis workflow into process steps, wherein within each process step all system parameters can be controlled and monitored. For a PET tracer synthesis, a sequence of process steps can be programmed, saved, loaded and modified, enabling full design flexibility to the operator. Sequences can be executed automatically or between user-defined breakpoints with the option of process step or sequence modifications "on the fly".

Proof-of-concept for SiFA radiochemistry

The radiolabeling of a PET tracer according to the SiFA method was chosen as the proof-of-concept example. The SiFA approach allows for a highly efficient isotopic exchange reaction that simplifies the synthesis workflow by enabling cartridge-based drying of fluoride-18.[76–80]

Bombesin analogues are imaging probes for oncological applications. They are ligands of the gastrin-releasing-peptide receptor (GRP-R) which is overexpressed on several tumor tissues such as prostate, breast, ovarian, lung, colon and gastrinoma cancers and therefore a feasible target structure for tumor visualization with PET.[81–83] The Bombesin derivative PESIN was tagged with a SiFA moiety and radiolabeled on the microfluidic platform according to the following steps:

(1) loading of all reagents including aqueous fluoride-18 activity from vials; (2) fluoride-18 phase transfer from aqueous to aprotic reaction conditions; (3) radiolabeling; (4) purification; and (5) ejection of the radiolabelled [^{18}F]PESIN PET tracer into a product vial.

Results

Microfluidic chip

Depending on microfluidic structure complexity, the total milling time per chip layer including loading and unloading of blanks varied between 20 min and 120 min. Without further optimization, the thermal bonding time was adjusted to 45 min and yielded chips without delamination defects. In

this way, different chip designs can be explored rapidly during chip development with high degrees of design flexibility for interconnecting valves, resins, reactors and I/O ports on-chip. For economy of scale, improvements can be achieved by customized injection moulding and solvent assisted bonding for rapid and cost effective chip manufacturing.

During and after handling of acetonitrile, DMF, DMSO or ethanol on-chip, no change in material color, transparency, material abrasion or swelling was observed. No significant chemical interaction was found between the chip material and the fluoride-18 radioactivity nor any other reagent or intermediate product utilized during the radiosynthesis described. Several test chips were operated at up to 140 °C resulting in no structural defects. This is consistent with results reported in previous studies for DMSO at 113 °C and HCl (1 M) at 80 °C.[84]

On-chip valve

Valve test structure fatigue was measured at an average gas pressure load of 5.8 bar (min. 4.1 bar, max. 6.2 bar, standard deviation 0.6 bar, 44 samples, pressure ramp up time 320 s ± 30 s). Improvements in increased pressure capabilities can be achieved by a further reduction of the valve diameter below 6 mm.

Valve cycle tests resulted in zero valve failure over 50 switching cycles (n = 37 valves from 8 different test chips investigated), which is the maximum load estimated for a single PET tracer synthesis run on a chip-based consumable. No change or cycle dependent drift was detected for the closing force or the gas flow rate across the open valve. This suggests that the valve functionality is not significantly affected by wearing effects such as membrane damage or valve seat deformation over 50 cycles.

During gas leakage measurements, no gas bubble formation could be detected over a 1.0 min measurement time, suggesting a gas leakage rate <0.1 μl min^{-1} at 2 bar gas pressure and 4 N closing force on the valve plunger.

On-chip resin

For the evaluation of on-chip resin performance, insert elements were packed with the anion exchange resin material from conventional cartridges (Sep-Pak® Light QMA Carbonate, part no. 186004540, Waters Corp.) and bonded into dedicated test chips by the method described. Fig. 5 shows a cross-section of an on-chip QMA resin. The boundaries between each insert element and the chip substrate material after bonding are partially optically transparent, suggesting a very good bond in these areas. The mechanical coupling between the insert and the substrate can be understood as a labyrinth sealing with the liquid pressure barrier significantly above the actual pressure drop across the regular fluid path through the cartridge. For cartridge functionality demonstration, the first steps of the [^{18}F]PESIN protocol were executed including fluoride-18 trapping, drying and subsequent release into a vial. For this process, the overall fluoride-18

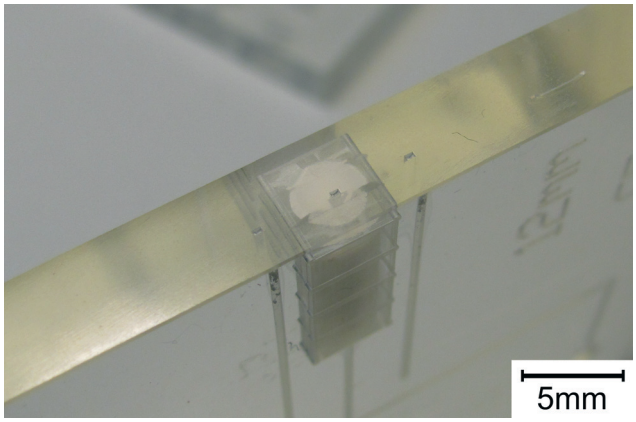

Fig. 5 Cross-section of a QMA resin for 18-fluoride drying integrated on a COC 6017 microfluidic chip.

losses were measured to be <11% (n = 3, decay corrected to start of experiment) and are comparable to conventional cartridge performance. However, an increased pressure drop across the on-chip cartridge of 1 bar to 3 bar higher than the conventional equivalent cartridge was measured. Since the resin geometry was kept comparable (L: 12 mm, B: 5 mm, H: 5 mm, bore diameter ø 4 mm, 46 mg resin), the results suggest a deformation of the insert element and a subsequent compression of the resin during bonding. This effect could be compensated by an appropriate tolerance design between the insert size and the on-chip recess size prior to bonding as outlined before.

Reagent loading

The transfer efficiency of aqueous fluoride-18 from the vial to chip according to the described gas pressurization method for starting volumes ranging from 100 μl to 500 μl at initial activities between 386 MBq (10.4 mCi) to 720 MBq (19.5 mCi) was measured at an average of 97.8% (max. 99.6%, min. 93.5%, standard deviation 1.6%, 17 samples), based on the comparison of vial activity before and after fluoride-18 loading to chip, decay corrected to the start of the experiment. Being the easiest quantifiable reagent for reagent transfer characterization, the aqueous 18-fluoride loading shows the efficiency of the presented approach and suggests a good transfer of the other vial supplied reagents utilized in the process. In fact, no synthesis failures from a lack of *e.g.* precursor or oxalic acid in the process could be detected.

Chemistry results

The total process efficiency, which is described by the fraction of fluoride-18 activity transferred from the starting vial (start of synthesis, SOS) into the purified [^{18}F]PESIN product, yielded 33% (±3%) (n = 4, not decay corrected) at >99% radiochemical purity (Agilent 1200 radio-HPLC, Agilent Technologies Inc., USA) with starting activities between 243 MBq (6.6 mCi) and 394 MBq (10.6 mCi). This overall efficiency is slightly below the manual equivalent process (approx. 40%

overall efficiency at >99% radiochemical purity, not decay corrected). The total process time was optimized to 36 min. Residual activity on-chip after synthesis completion without optimization of on-chip structures nor use of wash protocols was measured to be <14% across all runs (decay corrected to SOS). The described results were accomplished for a chip design with cartridges external to the chip, connected *via* capillary tubing across the described connector interface.

In a separate proof-of-concept experiment, both cartridges were transferred on-chip while maintaining the remaining chip design identical to the previous experiment (Fig. 6). This resulted in an overall process efficiency of 12% (not decay corrected) at >99% radiochemical purity in the first run. This is comparable to the early performance of the cartridge off-chip setup prior to chemistry protocol optimization.

The discrepancy results from the previously described on-chip resin compression during bonding which led to incorrect timing for mixing of reagents on-chip. This can be addressed by chemistry protocol optimization and improved cartridge insert design, suggesting that performance comparable to conventional processing is achievable.

Platform hardware

During test and evaluation of the microfluidic chemistry platform for the SiFA chemistry, chips have been successfully loaded and unloaded into the automated hardware over more than 100 cycles. Occasional leakage of the Tefzel Ferrules at the I/O ports due to deformation of the ferrule could be addressed by simple ferrule replacement. Even though the chips are design as single use disposable, they were used multiple times in case cartridges were off-chip. Gas pressure test protocols have been employed to ensure system functionality prior to the start of a synthesis. The platform was easy to move between fume hoods, hot cells and test sites in Europe and the United States at an average setup time of <30 min. after relocation. Radiochemistry users could be trained to operate the system within approx. one week.

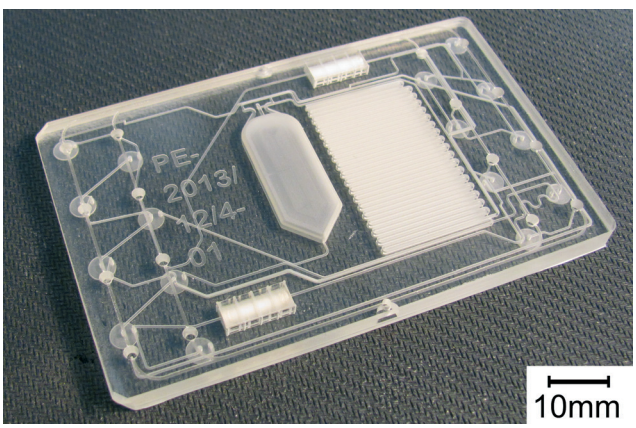

Fig. 6 The microfluidic chip for complete [^{18}F]PESIN synthesis with valves, reactors, QMA and SPE resins integrated on-chip.

Conclusion

With the recent FDA approval of new radiotracers for diagnosis of Alzheimer's disease such as Vizamyl™ (GE Healthcare, USA) and Amyvid™ (Eli Lilly, USA), the development of compact cyclotrons (ABT Molecular Imaging, Inc., Louisville, TN, USA[85] and PETtrace 600 prototype, GE Healthcare, Uppsala, Sweden) and integrated quality control systems for PET tracer production (QC1, Münster, Germany), the area is more vibrant than ever before.

Cost per PET tracer dose is the main driver towards PET imaging for small and de-central hospitals worldwide. Hence, the objective of this study is not to demonstrate microfluidic effects that push radiochemistry reactions to the extreme, which is another reason why microfluidics is of interest in this field, but rather develop an overall system solution that fundamentally enables cost saving microfluidic technologies to the clinical routine. Entering the development based on process compatible COC materials, the resulting chip maintains compatibility to large scale manufacturing by means of injection moulding and integration of all functional elements required for a simple PET tracer synthesis workflow. Pragmatic but viable solutions have been presented for on-chip valve and on-chip resin integration. Interfacing to "the macroworld", the microfluidic chip has been made accessible by a hardware interface that enables a reliable and automated chip exchange. The fully automated synthesis of the PET tracer [^{18}F]PESIN has been successfully implemented as a proof-of-concept study at yields close to the conventional process. Due to its compactness, the microfluidic radiochemistry platform including all hardware components can be easily relocated while providing a system architecture which is fundamentally compatible to very compact "self-shielded" designs. In its current state and with the prototype manufacturing for chips established, the platform is ready for field tests with academic partners around the globe in order to implement new PET tracer synthesis routines. Looking beyond applications in PET radiochemistry, the presented microfluidic chemistry platform can be extended to other areas in chemistry and biology that require chip consumables with high temperature and aggressive chemistry requirements.

Acknowledgements

The authors gratefully acknowledge the financial support from the Leading-Edge Cluster m4 and the German Federal Ministry of Education and Research. Special thanks to Arnaud Sors, Johannes Hass, Qing (Phoenix) Ba, Eva Bartok, Eric Simon, Jing Meng, Yue Wang and Andre Yaroshenko for their individual contribution.

References

1 M. E. Phelps, *Proc. Natl. Acad. Sci. U. S. A.*, 2000, **97**, 9226–9233.

2 V. Arima, G. Pascali, O. Lade, H. Kretschmer, I. Bernsdorf, V. Hammond, P. Watts, F. De Leonardis, M. Tarn, N. Pamme, P. S. Dittrich, B. Z. Cvetkovic, N. Vasovic, R. Duane, A. Jaksic, A. Zacheo, A. Zizzari, L. Marra, E. Perrone, P. Salvadori and R. Rinaldi, *Lab Chip*, 2013, **13**, 2328–2336.
3 H. Audrain, *Angew. Chem., Int. Ed.*, 2007, **46**, 1772–1775.
4 A. M. Elizarov, *Lab Chip*, 2009, **9**, 1326–1333.
5 R. Fortt and A. Gee, *Future Med. Chem.*, 2013, **5**, 241–244.
6 J. M. Gillies, C. Prenant, G. N. Chimon, G. J. Smethurst, B. A. Dekker and J. Zweit, *Appl. Radiat. Isot.*, 2006, **64**, 333–336.
7 P. Y. Keng, M. Esterby and R. M. van Dam, *Positron Emission Tomography - Current Clinical and Research Aspects*, ed. C.-H. Hsieh, InTech, New York, USA, 1st edn, 2012, pp. 153–182.
8 S. Y. Lu and V. W. Pike, in *PET chemistry: The driving force in molecular imaging*, ed. P. A. Schubiger, L. Lehmann and M. Friebe, Springer Verlag, Berlin, Germany, 2006, pp. 271–289.
9 E. Liow, A. O'Brien, S. Luthra, F. Brady and C. Steel, *J. Labelled Compd. Radiopharm.*, 2005, **48**, 28.
10 P. W. Miller, A. J. deMello and A. D. Gee, *Curr. Radiopharm.*, 2010, **3**, 254–262.
11 G. Pascali, P. Watts and P. A. Salvadori, Microfluidics in radiopharmaceutical chemistry, *Nucl. Med. Biol.*, 2013, **40**(6), 776–787.
12 C. K.-F. Shen, Microfluidic-assisted Radiochemistry and PET Probe Synthesis, *MI Gateway*, 2011, **5**(4), 1–5.
13 M. W. Wang, W. Y. Lin, K. Liu, M. Masterman-Smith and K. F. C. Shen, *Mol. Imaging*, 2010, **9**, 175–191.
14 E. Briard, S. S. Zoghbi, F. G. Siméon, M. Imaizumi, J. P. Gourley, H. U. Shetty, S. Lu, M. Fujita, R. B. Innis and V. W. Pike, *J. Med. Chem.*, 2009, **52**, 688–699.
15 G. Pascali, G. Mazzone, G. Saccomanni, C. Manera and P. A. Salvadori, *Nucl. Med. Biol.*, 2010, **37**, 547–555.
16 H. J. Wester, B. W. Schoultz, C. Hultsch and G. Henriksen, *Eur. J. Nucl. Med. Mol. Imaging*, 2009, **36**, 653–658.
17 P. Y. Keng, S. Chen, H. Ding, S. Sadeghi, G. J. Shah, A. Dooraghi, M. E. Phelps, N. Satyamurthy, A. F. Chatziioannou, C. J. Kim and R. M. van Dam, *Proc. Natl. Acad. Sci. U. S. A.*, 2012, **109**, 690–695.
18 A. M. Elizarov, M. R. van Dam, S. S. Young, H. C. Kolb, H. C. Padgett, D. Stout, J. Shu, J. Huang, A. Daridon and J. R. Heath, *J. Nucl. Med.*, 2010, **51**, 282–287.
19 C. Lee, G. Sui, A. M. Elizarov, C. J. Shu, Y. Shin, A. N. Dooley, J. Huang, A. Daridon, P. Wyatt, D. Stout, H. C. Kolb, O. N. Witte, N. Satyamurthy, J. R. Heath, M. E. Phelps, S. R. Quake and H. R. Tseng, *Science*, 2005, **310**, 1793–1796.
20 K. Liu, E. J. Lepin, M. W. Wang, F. Guo, W. Y. Lin, Y. C. Chen, S. J. Sirk, S. Olma, M. E. Phelps, X. Z. Zhao, H. R. Tseng, M. R. van Dam, A. M. Wu and C. K. Shen, *Mol. Imaging*, 2010, **10**, 168–176.
21 P. W. Miller, *J. Chem. Technol. Biotechnol.*, 2009, **84**, 309–315.
22 S. Chen, M. R. Javed, H.-K. Kim, J. Lei, M. Lazari, G. J. Shah, R. M. van Dam, P.-Y. Keng and C.-J. Kim, *Lab Chip*, 2014, **14**, 902–910.
23 R. Bejot, A. M. Elizarov and E. Ball, *J. Labelled Compd. Radiopharm.*, 2011, **54**, 117–122.
24 V. R. Bouvet, M. Wuest, P. H. Tam, M. Wang and F. Wuest, *Bioorg. Med. Chem. Lett.*, 2012, **22**, 2291–2295.
25 V. R. Bouvet, M. Wuest, L. I. Wiebe and F. Wuest, *Nucl. Med. Biol.*, 2011, **38**, 235–245.
26 S. Chen, R. Javed, J. Lei, H. K. Kim, G. Flores, R. M. van Dam, P. Y. Keng and C. J. Kim, *Technical Digest of the Solid-State Sensor and Actuator workshop*, Hilton Head Island, SC, June 3–7, 2012, pp. 189–192.
27 T. Collier, M. Akula and G. Kabalka, *J. Nucl. Med.*, 2010, **51**, 1462.
28 F. De Leonardis, G. Pascali, P. A. Salvadori, P. Watts and N. Pamme, Microfluidic modules for [$^{18}F^{-}$] activation – Towards an integrated modular lab on a chip for PET radiotracer synthesis, *Proc. MicroTAS*, 2010, 1604–1606.
29 V. Gaja, V. Gomez-Vallejo, M. Cuadrado-Tejedor, J. I. Borrell and J. Llop, *J. Labelled Compd. Radiopharm.*, 2012, **55**, 332–338.
30 J. M. Gillies, C. Prenant, G. N. Chimon, G. J. Smethurst, W. Perrie, I. Hamblett, B. Dekker and J. Zweit, *Appl. Radiat. Isot.*, 2006, **64**, 325–332.
31 S. Kealey, C. Plisson, T. L. Collier, N. J. Long, S. M. Husbands, L. Martarello and A. D. Gee, *Org. Biomol. Chem.*, 2011, **9**, 3313–3319.
32 A. Lebedev, R. Miraghaie, K. Kotta, C. E. Ball, J. Zhang, M. S. Buchsbaum, H. C. Kolb and A. M. Elizarov, *Lab Chip*, 2013, **13**, 136–145.
33 S. Y. Lu, P. Watts, F. T. Chin, J. Hong, J. L. Musachio, E. Briard and V. W. Pike, *Lab Chip*, 2004, **4**, 523–525.
34 S. Y. Lu, A. M. Giamis and V. W. Pike, *Curr. Radiopharm.*, 2009, **2**, 49–55.
35 S. Y. Lu and V. W. Pike, *J. Fluorine Chem.*, 2010, **131**, 1032–1038.
36 P. W. Miller, H. Audrain, D. Bender, A. J. deMello, A. D. Gee, N. J. Long and R. Vilar, *Chem. – Eur. J.*, 2011, **17**, 460–463.
37 G. Pascali, G. Nannavecchia, S. Pitzianti and P. A. Salvadori, *Nucl. Med. Biol.*, 2011, **38**, 637–644.
38 C. Rensch, B. Waengler, A. Yaroshenko, V. Samper, M. Baller, N. Heumesser, J. Ulin, S. Riese and G. Reischl, *Appl. Radiat. Isot.*, 2012, **70**, 1691–1697.
39 S. V. Selivanova, L. Mu, J. Ungersboeck, T. Stellfeld, S. M. Ametamey, R. Schibli and W. Wadsak, *Org. Biomol. Chem.*, 2012, **10**, 3871–3874.
40 C. J. Steel, A. T. O'Brien, S. K. Luthra and F. Brady, *J. Labelled Compd. Radiopharm.*, 2007, **50**, 308–311.
41 R. W. Simms, P. W. Causey, D. M. Weaver, C. Sundararajan, K. A. Stephenson and J. F. Valliant, *J. Labelled Compd. Radiopharm.*, 2012, **55**, 18–22.
42 J. Ungersboeck, S. Richter, L. Collier, M. Mitterhauser, G. Karanikas, R. Lanzenberger, R. Dudczak and W. Wadsak, *Nucl. Med. Biol.*, 2012, **39**, 1087–1092.
43 J. Ungersboeck, C. Philippe, L. K. Mien, D. Haeusler, K. Shanab, R. Lanzenberger, H. Spreitzer, B. K. Keppler, R. Dudczak, K. Kletter, M. Mitterhauser and W. Wadsak, *Nucl. Med. Biol.*, 2011, **38**, 427–434.

44 J. Ungersboeck, C. Philippe, D. Haeusler, M. Mitterhauser, R. Lanzenberger, R. Dudczak and W. Wadsak, *Appl. Radiat. Isot.*, 2012, **70**, 2615–2620.
45 S. Voccia, J. L. Morelle, J. Aerts, C. Lemaire, A. Luxen and G. Phillipart, *J. Labelled Compd. Radiopharm.*, 2009, **52**, i–xliii.
46 T. D. Wheeler, D. X. Zeng, A. V. Desai, B. Onal, D. E. Reichert and P. J. A. Kenis, *Lab Chip*, 2010, **10**, 3387–3396.
47 D. L. Yokell, A. K. Leece, A. A. Lebedev, R. R. Miraghaie, C. E. Ball, J. J. Zhang, H. C. Kolb, A. M. Elizarov and U. U. Mahmood, *Appl. Radiat. Isot.*, 2012, **70**, 2313–2316.
48 D. Zeng, A. V. Desai, D. Ranganathan, T. D. Wheeler, P. J. A. Kenis and D. E. Reichert, *Nucl. Med. Biol.*, 2013, **40**, 42–51.
49 C. Rensch, A. Jackson, S. Lindner, R. Salvamoser, V. Samper, S. Riese, P. Bartenstein, C. Wängler and B. Wängler, *Molecules*, 2013, **18**, 7930–7956.
50 R. G. Zimmermann, *Nucl. Med. Biol.*, 2013, **40**, 155–156.
51 U. M. Attia, S. Marsona and J. R. Alcockb, *Microfluid. Nanofluid.*, 2009, **7**, 1–28.
52 J. Steigert, S. Haeberle, T. Brenner, C. Müller, C. P. Steinert, P. Koltay1, N. Gottschlich, H. Reinecke, J. Rühe, R. Zengerle and J. Ducrée, *J. Micromech. Microeng.*, 2007, **17**, 333–341.
53 H.-J. Machulla, A. Blocher, M. Kuntzsch, M. Piert, R. Wei and J. R. Grierson, *J. Radioanal. Nucl. Chem.*, 2000, **243**, 843–846.
54 M. A. Unger, H. P. Chou, T. Thorsen, A. Scherer and S. R. Quake, *Science*, 2000, **288**, 113–116.
55 C. F. Chen, J. Liu, C.-C. Chang and D. L. DeVoe, *Lab Chip*, 2009, **9**, 3511–3516.
56 I. R. G. Ogilvie, V. J. Sieben, B. Cortese, M. C. Mowlem and H. Morgan, *Lab Chip*, 2011, **11**, 2455–2459.
57 M. Bu, I. R. Perch-Nielsen and Y. Sun, *et al.*, in *Digest of Technical Papers: Transducers 2011*, Beijing, China, 2011, pp. 1244–1247.
58 K. W. Oh and C. H. Ahn, *J. Micromech. Microeng.*, 2006, **16**, R13–R39.
59 V. D. Samper, C. Rensch, C. Boeld and M. Baller, *Patent application*, WO2011082276/A1, 2011.
60 F. De Leonardis, G. Pascali, P. A. Salvadori, P. Watts and N. Pamme, *J. Chromatogr. A*, 2011, **1218**, 4714–4719.
61 R. Ismail, K.-J. Park, M. R. van Dam and P. Keng, *J. Nucl. Med.*, 2012, **53**, 572.
62 K. Hamacher, T. Hirschfelder and H. H. Coenen, *Appl. Radiat. Isot.*, 2002, **56**, 519–523.
63 K. Hamacher and H. H. Coenen, *Appl. Radiat. Isot.*, 2006, **64**, 989–994.
64 D. Alexoff, D. J. Schlyer and A. P. Wolf, *Appl. Radiat. Isot.*, 1989, **40**, 1–6.
65 G. Reischl, W. Ehrlichmann and H.-J. Machulla, *J. Radioanal. Nucl. Chem.*, 2002, **254**, 29–31.
66 R. Wong, R. Iwata, H. Saiki, S. Furumoto, Y. Ishikawa and E. Ozeki, *Appl. Radiat. Isot.*, 2012, **70**, 193–199.
67 H. Saiki, R. Iwata, H. Nakanishi, R. Wong, Y. Ishikawa, S. Furumoto, R. Yamahara, K. Sakamoto and E. Ozeki, *Appl. Radiat. Isot.*, 2010, **68**, 1703–1708.
68 F. Saito, Y. Nagashima, A. Goto, M. Iwaki, N. Takahashi, T. Oka, T. Inoue and T. Hyodo, *Appl. Radiat. Isot.*, 2007, **65**, 524–527.
69 S. Sadeghi, V. Liang, S. Cheung, S. Woo, C. Wu, J. Ly, Y. Deng, M. Eddings and R. M. van Dam, *Appl. Radiat. Isot.*, 2013, **75C**, 85–94.
70 B. Cvetkovic, O. Lade, L. Marra, V. Arima, R. Rinaldi and P. S. Dittrich, *RSC Adv.*, 2012, **29**, 11117–11122.
71 M. R. Javed, S. Chen, H.-K. Kim, L. Wei, J. Czernin, C.-J. Kim, R. M. van Dam and P. Y. Keng, *J. Nucl. Med.*, 2014, **55**, 1–8.
72 J. Billen and G. Desmet, *J. Chromatogr. A*, 2007, **1168**, 73–99.
73 C. K. Fredrickson and Z. H. Fan, *Lab Chip*, 2004, **4**, 526–533.
74 M. K. Baller, V. D. Samper and C. Rensch, *Patent application*, WO2012/015856A1, 2012.
75 C. Boeld, V. D. Samper, C. Rensch and R. J. Salvamoser, *Patent application*, US2012/0024405, 2012.
76 C. Wängler, S. Niedermoser, J. Chin, K. Orchowski, E. Schirrmacher, K. Jurkschat, L. Iovkova-Berends, A. P. Kostikov, R. Schirrmacher and B. Wängler, *Nat. Protoc.*, 2012, **7**, 1946–1955.
77 C. Wängler, A. Kostikov, J. Zhu, J. Chin, B. Wängler and R. Schirrmacher, *Appl. Sci.*, 2012, **2**, 277–302.
78 C. Wängler, B. Waser, A. Alke, L. Iovkova, H. G. Buchholz, S. Niedermoser, K. Jurkschat, C. Fottner, P. Bartenstein, R. Schirrmacher, J. C. Reubi, H. J. Wester and B. Wängler, *Bioconjugate Chem.*, 2010, **21**, 2289–2296.
79 R. Schirrmacher, G. Bradtmöller, E. Schirrmacher, O. Thews, J. Tillmanns, T. Siessmeier, H. G. Buchholz, P. Bartenstein, B. Wängler, C. M. Niemeyer and K. Jurkschat, *Angew. Chem., Int. Ed.*, 2006, **45**, 6047–6050.
80 E. Schirrmacher, B. Wängler, M. Cypryk, G. Bradtmöller, M. Schäfer, M. Eisenhut, K. Jurkschat and R. Schirrmacher, *Bioconjugate Chem.*, 2007, **18**, 2085–2089.
81 J. C. Reubi, S. Wenger, J. Schmuckli-Maurer, J.-C. Schaer and M. Gugger, *Clin. Cancer Res.*, 2002, **8**, 1139–1146.
82 D. Cornelio, R. Roesler and G. Schwartsmann, *Ann. Oncol.*, 2007, **18**, 1457–1466.
83 V. Ambrosini, M. Fani, S. Fanti, F. Forrer and H. R. Maecke, *J. Nucl. Med.*, 2011, **52**, 42S–55S.
84 C. Rensch, B. Wängler, C. Boeld, M. Baller, V. Samper, N. Heumesser, W. Ehrlichmann, S. Riese and G. Reischl, *J. Nucl. Med.*, 2011, **52**, 288.
85 V. Awasthia, J. Watsonb, H. Galia, G. Matlocka, A. McFarlandb, J. Baileyb and A. Anzellottib, *Appl. Radiat. Isot.*, 2014, **89**, 167–175.

